Korean J. Chem. Eng., 34(7), 1914-1923 (2017)
DOI: 10.1007/s11814-017-0097-y

pISSN: 0256-1115
eISSN: 1975-7220

Heterogeneous amino acid-based tungstophosphoric acids as efficient and recyclable catalysts for selective oxidation of benzyl alcohol

Xiaoxiang Han*,†, Yingying Kuang*, Chunhua Xiong*, Xiujuan Tang, Qing Chen*, Chin-Te Hung***, Li-Li Liu***, and Shang-Bin Liu***,†**

*Department of Applied Chemistry, Zhejiang Gongshang University, Hangzhou 310018, China
**College of Environmental Science and Engineering, Zhejiang Gongshang University, Hangzhou 310018, China
***Institute of Atom and Molecular Sciences, Academic Sinica, Taipei 10617, Taiwan
(*Received 29 November 2016 • accepted 4 April 2017*)

Abstract−A series of organic-inorganic composite catalysts, prepared by modifying tungstophosphoric acid (TPA; $H_3PW_{12}O_{40}$) with different amino acids such as phenylalanine (Phe), alanine (Ala), and glycine (Gly) were synthesized. The physicochemical and acidic properties of these $(MH)_xH_{3-x}PW_{12}O_{40}$ (M=Phe, Ala, and Gly; x=1-3) composite materials were characterized by a variety of different analytical and spectroscopic techniques, namely TGA, XRD, FT-IR, XPS, and NMR, and exploited as heterogeneous catalysts for selective oxidation of benzyl alcohol (BzOH) with hydrogen peroxide (H_2O_2). Among them, the $[PheH]H_2PW_{12}O_{40}$ catalyst exhibited the best oxidative activity with an excellent BzOH conversion of 99.0% and a desirable benzaldehyde (BzH) selectivity of 99.6%. Further kinetic studies and model analysis by response surface methodology (RSM) revealed that the oxidation of BzOH with H_2O_2 follows a second-order reaction with an activation energy of 56.7 kJ·mol^{-1} under optimized experimental variables: BzOH/H_2O_2 molar ratio=1 : 1.5 mol/mol, amount of catalyst=6.1 wt%, reaction time (x_3)=3.8 h, and amount of water (x_4)=30.2 mL.

Keywords: Amino Acid, Heteropolyacid, Benzaldehyde, Oxidation of Alcohol, Process Optimization, Kinetic Model

INTRODUCTION

Aldehydes and ketones are common and versatile flavoring agents for the food, beverage, fragrance, and pharmaceutical industries, thus, are of great market perspectives. As such, the selective oxidation of alcohols to aldehydes, ketones, and other carbonyl compounds alike is an essential process in organic chemistry for academic research as well as industrial productions [1]. Recently, the utilization of hydrogen peroxide (H_2O_2) as an oxidant during selective oxidation of alcohols to carbonyls has drawn considerable R&D attentions [2-6]. This is owing to the fact that such reaction is not only highly efficient but also green and economical, with water as the sole by-product.

Owing to the super acidic, highly soluble (in polar solvents), low volatility, non-toxic, redox, and pseudoliquid characteristics, heteropolyacids (HPAs) are useful, versatile, and eco-friendly catalysts for acid-catalyzed reactions in both homogeneous and heterogeneous systems [7-11]. Nonetheless, formidable recovery and reuse and ineffective catalytic activity due to low surface area (typically $<10\ m^2\ g^{-1}$) largely limit their applications, especially in homogeneous reaction system. To unravel these drawbacks, extensive efforts have been made in developing novel HPA-based solid acid catalysts, for examples, by anchoring HPA on porous supports or by combining them with desirable organic compounds to form organic-inorganic composites while preserving the strong acidic property to sustain a high catalytic activity [12-21]. For instance, metal ion-exchanged HPAs [8,22-24] and amino-functionalized HPAs [25, 26] have been exploited in many chemical reactions, including the oxidation of benzyl alcohol. These multifunctional HPA-based catalysts not only exhibit excellent catalytic properties but also unique physicochemical properties such as temperature-tolerant, low-cost, environmentally-benign, and excellent separation and recyclability [27-29].

Amino acids, being the structural units of proteins, are important organic compounds containing amine (-NH_2) and carboxyl (-COOH) functional groups. Thus, amino acid-modified HPAs represent a new type of non-toxic organic-inorganic composites, which are cost-effective, eco-friendly, and recyclable acid catalysts for catalytic conversions of biomass, for examples, conversion of glucose to 5-hydroxymethylfurfural (HMF) or levulinic acid (LA) [25], oxidation of alcohol [26] and esterification of palmitic acid to biodiesel [30]. In view of the fact that few research report on oxidation of alcohols were made over amino acid-functionalized HPAs, herein, we report the synthesis of a series of different amino acid functionalized tungstophosphoric acid (TPA) composite materials; the adopted amino acids include phenylalanine (Phe), alanine (Ala), and glycine (Gly). The amino acid-modified TPA catalysts so prepared, namely $(MH)_xH_{3-x}PW_{12}O_{40}$ (M=Phe, Ala, and Gly; x=1-3) were characterized by a variety of physicochemical techniques, including TGA, XRD, FT-IR, XPS, and ^1H and ^{13}C NMR. In particular, their acidic properties were investigated by solid-state ^{31}P magic-angle-spinning (MAS) NMR using the adsorbed trialkylphosphine oxide (TMPO) as the probe molecule [31,32]; *i.e.*, the ^{31}P-TMPO NMR acidity characterization approach. These organic-inorganic

†To whom correspondence should be addressed.
E-mail: hxx74@126.com, sbliu@sinica.edu.tw

composite catalysts were exploited for selective oxidation of benzyl alcohol (BzOH) with hydrogen peroxide (H_2O_2). Based on the Box-Behnken design (BBD), the effects of different experimental variables, namely BzOH/H_2O_2 molar ratio, amount of catalyst, reaction time, and amount of water on catalytic activities during the oxidation reaction were optimized by response surface methodology (RSM). Moreover, analysis of variance (ANOVA) was employed to investigate the interactions between pair of experimental variables and their effects on the catalytic process. A kinetic model of the oxidation reaction was also established and assessed based on the optimal reaction conditions.

EXPERIMENTAL

1. Catalyst Preparation

The organic-inorganic composite catalysts were prepared following the procedures reported elsewhere [30]. In brief, equal amount of tungstophosphoric acid (TPA; $H_3PW_{12}O_{40}$) and desirable amino acid, namely phenylalanine (Phe), alanine (Ala), and glycine (Gly), were first dissolved in water, then, the mixed solution was allow to stir at 90 °C overnight. After water removal, the solid product was washed with diethyl ether followed by drying under vacuum. The product so obtained are denoted as $[MH]H_2PW_{12}O_{40}$ (M=Phe, Ala, and Gly; see Table 1). For comparison, the Phe series samples, namely $[PheH]_xH_{3-x}PW_{12}O_{40}$, were prepared by varying the molar ratios of Phe/TPA, *viz.* 0, 1/3, 2/3, and 1 (*i.e.*, x=0-3). All research grade chemicals were used without further purification unless specified otherwise.

2. Catalyst Characterization

All Fourier-transform infrared (FT-IR) experiments were performed following the conventional KBr pellet procedure on a Bruker IFS-28 spectrometer. Each FT-IR spectrum was recorded by accumulating 32 scans within a range of 400-4,000 cm^{-1} with a resolution of 1 cm^{-1}. Sample surface properties were investigated by X-ray photoelectron spectroscopy (XPS) using an electron spectrometer (ESCALab220i-XL; VG Scientific) via 300 W Al Kα radiation. The base pressure was kept at 3×10^{-9} mbar and the binding energies were referenced to adventitious carbon C1s XPS peak at 284.6 eV. Sample structural properties were study by powdered X-ray diffraction (XRD) conducted on a Bruker D8 ADVANCE X-ray diffractometer equipped with a Ni-filtered Cu Kα radiation generated at 40 kV and 20 mA. Each XRD pattern was scanned over a 2θ angle of 5° to 80° at an interval of 0.02°. The thermal stability of the catalyst was characterized by a thermal gravimetric analyzer (TGA; Netzsch TG-209) under nitrogen atmosphere recorded within a range from room temperature (RT; 25 °C) to 600 °C at a ramp rate of 20 °C min^{-1}. High-resolution solution-state ^1H and ^{13}C nuclear magnetic resonance (NMR) spectra were obtained from samples dissolved in deuterated water (D_2O) and were acquired using a single-pulse sequence on a Bruker AV-500 spectrometer operated at a Larmor frequency of 500.130 and 125.758 MHz, respectively. The acid features (*i.e.*, type, concentration, and strength) of the solid acid catalysts were explored by means of the ^{31}P-TMPO NMR approach [31,32] using trimethylphosphine oxide (TMPO) as the probe molecule. Solid-state ^{31}P magic-angle spinning (MAS) NMR spectra of TMPO-adsorbed catalysts were acquired at a Larmor frequency of 202.457 MHz using a 4 mm double-resonance MAS probehead under the conditions: pulse-width 1.5 μs (π/6), recycle delay 10 s, sample spinning rate 12 kHz.

3. Catalytic Reaction

The catalytic activity of the various $[MH]_xH_{3-x}PW_{12}O_{40}$ (M=Phe, Ala, and Gly; x=0-3) composite catalysts were assessed by oxidation of benzyl alcohol (BzOH) with hydrogen peroxide (H_2O_2) to benzaldehyde (BzH). The reactions were performed in a three-necked flask (100 mL) connecting to a condenser. For each run, designated amounts of BzOH and H_2O_2 (30%) were placed in the reactor with a suitable amount of catalyst (3-8 wt%) and water (10-35 mL). Then, the reaction was carried out at a desirable temperature (90-130 °C) for a varied period of time (2-5 h). After the reaction, the reaction mixture was then cooled to room temperature to which two segregated layers were automatically formed. The product (top) and catalyst (bottom) layers were separated by extraction with ethyl acetate. The reaction products were analyzed by gas chromatography (GC; Agilent 6890B) equipped with a flame ionization detector (FID) and a HP-5 capillary column. The yield of product (benzaldehyde; BzH) was derived by:

$$\text{Yield (\%)}=\text{Conversion (\%)}\times\text{Selectivity (\%)}. \quad (1)$$

A typical GC profile of product compositions are illustrated in Fig. S1 of the Supplementary Information (SI).

4. Experimental Design and Mathematical Model

An experimental design for a series of experimental variables based on RSM (Design-Expert r Version 8.0.7.1) was used for the production of BzH by oxidation of BzOH over $[PheH]H_2PW_{12}O_{40}$. A Box-Behnken design (BBD) was utilized to study the effect of four independent process variables, namely BzOH/H_2O_2 molar ratio (x_1), amount of catalyst (x_2), reaction time (x_3), and amount of water (x_4). All factors in the experiment were established and coded into three levels −1, 0, and +1, as defined in Table 2. In addition, a 3^4 full-factorial central composite design with the three coded levels was utilized, for which 29 experimental sets (24 factorial and 5 central points) were adopted, as depicted in Table 3. The coded values of each independent variable were calculated by the equation:

Table 1. Catalytic performances of various catalysts during oxidation of benzyl alcohol with hydrogen peroxide[a]

Catalyst	Conversion (%)[b]	Product	
		Selectivity (%)[b]	Yield (%)[b]
Phe	Nil	Nil	Nil
$H_3PW_{12}O_{40}$	96.7	90.0	87.0
$[PheH]H_2PW_{12}O_{40}$	97.9	97.4	95.4
$[PheH]_2HPW_{12}O_{40}$	97.5	92.0	89.7
$[PheH]_3PW_{12}O_{40}$	96.3	91.8	88.4
$[AlaH]H_2PW_{12}O_{40}$	97.8	94.7	92.7
$[GlyH]H_2PW_{12}O_{40}$	97.7	92.9	90.8

[a]Reaction conditions: BzOH/H_2O_2=1 : 2 (mol/mol); amount of catalyst=6 wt%; reaction time=4 h; amount of water=30 mL; temperature 110 °C

[b]Analyzed by GC

Table 2. List of symbols for various experimental variables and corresponding coded levels and ranges adopted in the experimental design

Variable (unit)	Symbol	Range and level		
		−1	0	1
$BzOH/H_2O_2$ (mol/mol)	x_1	1 : 1	1 : 2	1 : 3
Catalyst loading (wt%)	x_2	5	6	7
Reaction time (h)	x_3	3	4	5
Amount of water (mL)	x_4	25	30	35

Table 3. List of experimental design and response values obtained for oxidation of benzyl alcohol over the $[PheH]H_2PW_{12}O_{40}$ catalyst

Entry	Variable and level				BzH yield (%)
	x_1	x_2	x_3	x_4	
1	−1	−1	0	0	95.67
2	1	−1	0	0	68.43
3	−1	1	0	0	93.25
4	1	1	0	0	68.69
5	0	0	−1	−1	94.34
6	0	0	1	−1	80.59
7	0	0	−1	1	94.46
8	0	0	1	1	91.15
9	−1	0	0	−1	95.16
10	1	0	0	−1	60.98
11	−1	0	0	1	95.13
12	1	0	0	1	73.34
13	0	−1	−1	0	94.22
14	0	1	−1	0	92.30
15	0	−1	1	0	89.33
16	0	1	1	0	88.99
17	−1	0	−1	0	96.24
18	1	0	−1	0	75.13
19	−1	0	1	0	95.26
20	1	0	1	0	56.29
21	0	−1	0	−1	87.48
22	0	1	0	−1	89.59
23	0	−1	0	1	87.17
24	0	1	0	1	96.40
25	0	0	0	0	96.00
26	0	0	0	0	95.94
27	0	0	0	0	93.62
28	0	0	0	0	94.46
29	0	0	0	0	97.39

$$x_i = \frac{X_i - X_0}{\Delta X_i} \quad (2)$$

where x_i (i=1-4) were the coded value of the independent variables, X_i, X_0, and DX_i (i=1-4) represent the real, central, step-change value of the associated variable, respectively.

Accordingly, the yield of the product yield (*i.e.*, BzH) and corresponding response of the experimental design, may be expressed as:

$$Y = \beta_0 + \sum_{i=1}^{4}\beta_i x_i + \sum_{i=1}^{4}\beta_{ii} x_i^2 + \sum_{i<j}^{4}\beta_{ij} x_i x_j \quad (3)$$

where x_i and x_j (i & j=1-4) denote the uncoded independent variables, while β_0, β_i, β_{ii}, and β_{ij} represent the regression coefficients for the corresponding variables. The validity and significance of the proposed model were assessed through statistical parameters based on ANOVA method.

5. Kinetic Study

The initial reaction rate method was exploited for studying the kinetics of the oxidation reaction conducted at different conditions to obtain the kinetic expression. In these experiments, different process variables such as $BzOH/H_2O_2$ ratio, reaction temperature, and so on were explored while the other parameters were kept constant. In this context, the reaction rate (r) for the oxidation of BzOH with H_2O_2 to BzH may be expressed by the following rate equation:

$$r = -dC_A/dt = k' C_A^{\alpha} C_B^{\beta} \quad (4)$$

where C_A and C_B represent the instant concentration of BzOH and H_2O_2, respectively, k′ is the rate constant, and α and β denote the reaction order corresponding to BzOH and H_2O_2, respectively. Taking the natural logarithm, Eq. (4) can further be expressed as:

$$\ln r = \ln k + \alpha \ln C_A \quad (5)$$

where $k = k' C_B^{\beta}$ represents the modified rate constant. Accordingly, the rate constant may be correlated with activation energy (E_a) by the Arrhenius equation:

$$\ln k = \ln k_0 - \frac{E_a}{R}\frac{1}{T} \quad (6)$$

where k_0 denotes the pre-exponential factor, R is the gas constant, and T represents the reaction temperature.

RESULTS AND DISCUSSION

1. Catalyst Properties

The FT-IR spectra of the pristine TPA ($H_3PW_{12}O_{40}$) exhibited seven characteristic stretching and vibrational bands anticipated for the Keggin structure. As shown in Fig. S2(b) (SI), the bands at 3,435, 1,080, 981, 889, 804, 598, and 516 cm^{-1} may be attributed to asymmetric stretching of O-H, P-O, terminal W=O, corner-sharing W-O_b-W, edge-sharing W-O_c-W, symmetric vibrations of O-P-O and W-O-W, respectively [14,30]. Upon incorporating phenylalanine (Phe) onto TPA, the characteristic bands remained present in the $[PheH]_xH_{3-x}PW_{12}O_{40}$ (x=1-3, see Figs. S2(c)-(e); SI) composite catalysts regardless of the slight decreases in peak intensity. This indicates that these organic-inorganic composite salts preserved their structural integrity of the polyanion $PW_{12}O_{40}^{3-}$ (PW) in the Keggin unit even after substituting protons (H^+) in TPA for the $[PheH]^+$ cations. Moreover, two additional bands were observed for the Phe-modified catalysts. These two bands at 3,159 and 1,614 cm^{-1} may be ascribed due to asymmetric stretching of N-H and stretching of COO^- in Phe, respectively, as may be verified by the characteristic IR bands observed for the pure Phe (Fig. S2(a); SI).

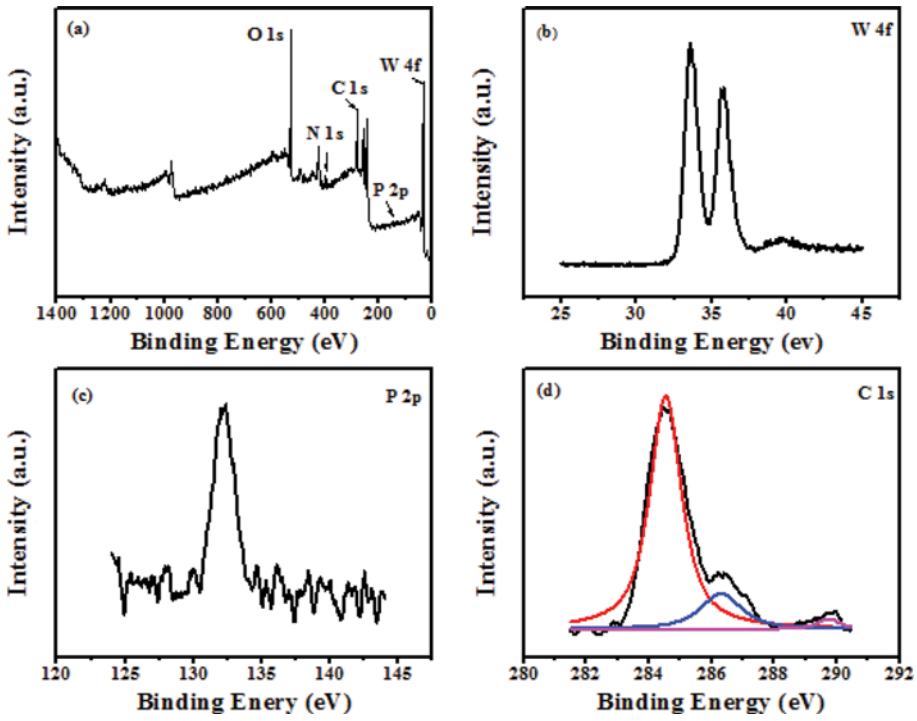

Fig. 1. XPS (a) survey spectrum and high-resolution spectra for the (b) W 4f, (c) P 2p, and (d) C 1s core levels of the $[PheH]H_2PW_{12}O_{40}$ catalyst.

The surface properties of the $[PheH]_xH_{3-x}PW_{12}O_{40}$ (x=1-3) catalysts were monitored by XPS spectroscopy. Fig. 1 displays the XPS spectra of the $[PheH]H_2PW_{12}O_{40}$ sample. As shown in the survey spectrum in Fig. 1(a), the N 1s peak responsible for the amino nitrogen of Phe gave rise to a binding energy of 402.5 eV higher than that of bulk Phe (401.7 eV) [33], indicating the successful incorporation of Phe onto the TPA. The XPS core level spectrum of W 4f (Fig. 1(b)) showed two distinct peaks at binding energy of 36.1 and 38.2 eV anticipated for the W 4f and W $4f_{7/2}$ spin-orbit components, respectively. Comparing to the bulk TPA, which exhibits two prominent peaks at 35.8 and 37.9 eV, the apparent energy shift observed for the $[PheH]H_2PW_{12}O_{40}$ reveals a change from the W=O to the W-O bond upon incorporating Phe onto TPA. Likewise, a notable shift was also observed for the P 2p singlet peak at 134.9 eV compared to the bulk TPA (136.0 eV). Moreover, the broad C 1s core-level spectrum may be deconvoluted into three bands with a binding energy of 290.1, 286.3, and 284.6 eV (Fig. 1(d)), accountable for the C=O, C-O, and C-C bonds, respectively [34,35]. The XPS results above therefore provide supporting evidences to confirm coupling of Phe with proton (on TPA) to form $[PheH]^+$, thus, the successful anchoring of Phe and formation of the $[PheH]H_2PW_{12}O_{40}$ composite catalyst (*vide infra*).

The structural properties of the amino acid-modified TPA were also investigated by powder XRD, as shown in Fig. S3 (SI). The pristine TPA, which displayed main diffraction peaks at 2θ of 10.3, 25.3, and 34.6° (Fig. S3(b); SI) expected for the signature of Keggin structure [36]. It is evident that these characteristic peaks also present in the $[PheH]_xH_{3-x}PW_{12}O_{40}$ (x=1-3) catalysts but with somewhat weaker peak intensities (Figs. S3(c)-(e); SI). Moreover, additional peaks associated with the incorporated Phe also emerged in the 2θ region of *ca.* 5-10° [37]. Again, results obtained from XRD measurements verify the successful anchoring of Phe onto the TPA.

The above findings are also supported by further high-resolution NMR and TGA measurements on $[PheH]_xH_{3-x}PW_{12}O_{40}$ (x= 0-3) series catalysts. As an illustration, the NMR data obtained for the $[PheH]H_2PW_{12}O_{40}$ catalyst are listed below: ^{1}H NMR (500 MHz, D_2O); δ 3.21 (d, 1H), 3.49 (d, 1H), 4.30 (t, 1H), 7.34 (m, 5H) ppm; ^{13}C NMR (500 MHz, D_2O); δ 35.80, 54.25, 128.22, 129.42, 129.58, 134.05, 171.36 ppm. Likewise, since all amino-acid modified TPA catalysts led to similar conclusions, here, only the thermogravimetry and derivative thermogravimetry (TG-DTG) curves of the $[PheH]H_2PW_{12}O_{40}$ sample are illustrated and discussed. As shown in Fig. S4(b) (SI), the pristine TPA exhibited three weight-loss peaks at 73, 195, and 530 °C, which may be attributed to weight-loss of physisorbed water, crystalline water, and collapsed Keggin structural unit, respectively. By comparison, bulk Phe showed a single weight-loss peak at *ca.* 270 °C (Fig. S4(a); SI) due to decomposition of Phe. On the other hand, three distinct weight-loss peaks at 170, 281, and 556 °C were observed for the $[PheH]H_2PW_{12}O_{40}$ catalyst (Fig. S4(c); SI). The former weight-loss peak may be attributed unambiguously to the loss of crystalline water, whereas the latter two peaks should be due to the decomposition of organic species and collapse of Keggin structure, respectively. Thus, results obtained from NMR and thermal analysis further demonstrate that the PW polyanions were indeed successfully anchored with Phe, and remained stable at the reaction temperature (≤130 °C) employed in the present study.

To afford information on acid properties of the as-prepared catalyst samples, we exploited the ^{31}P-TMPO MAS NMR approach [31,32], which is facilitated by linear dependence between the observed ^{31}P NMR chemical shift (δ^{31}P) of TMPO and strength of Brønsted acidity [38]. The ^{31}P NMR spectrum of TMPO adsorbed

on the pristine TPA typically shows multiple ^{31}P signals within two chemical shift ranges. The sharp ^{31}P resonances at located at *ca.* −10 and −15 ppm may be unambiguously ascribed due to PW polyanions of the TPA [36], whereas those within the range of 55-95 ppm due to TMPO adsorbed on Brønsted acid sites of the TPA catalyst [15,20,30,39]. It is noteworthy that the pristine TPA indeed possesses Brønsted acid sites with super acidity (i.e., those with $\delta^{31}P \geq 86$ ppm) [31,32,36,38], as revealed by the presences of ^{31}P resonance peaks at 82, 88, and 92 ppm (Fig. 2(a)) corresponding to TMPO adsorbed on the three available Brønsted H^+ sites (*i.e.*, $TMPOH^+$). Whereas the ^{31}P resonances located within 55-80 ppm due to $(TMPO)_nH^+$ (n≥2) species [36]. Upon incorporation of Phe, a notable decrease in acidic strength of the $[PheH]_xH_{3-x}PW_{12}O_{40}$ (x=1-3) catalysts was observed. This may be inferred by the gradual decrease in the $\delta^{31}P$ of adsorbed TMPO with increasing Phe loading (x). Note that Phe alone exhibited only very weak acidity with $\delta^{31}P$ at only 41 ppm. Thus, it is conclusive that the acidic strength of various samples follows the descending order: $H_3PW_{12}O_{40}$>> $[PheH]H_2PW_{12}O_{40}$>$[PheH]_2HPW_{12}O_{40}$>$[PheH]_3PW_{12}O_{40}$>>Phe.

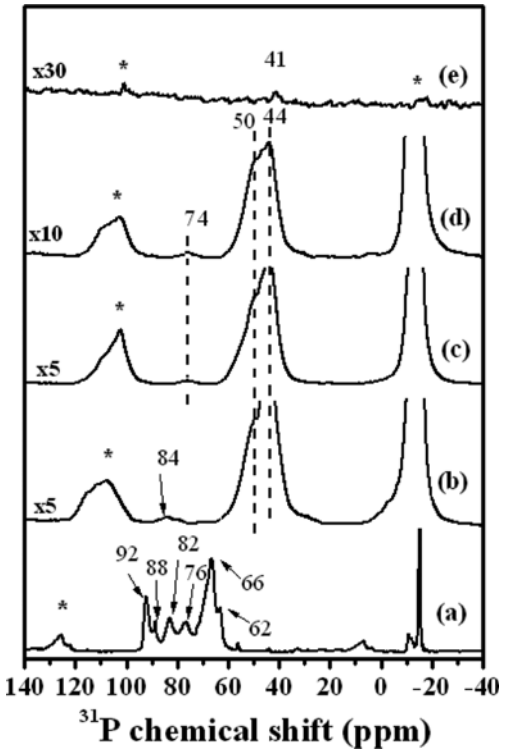

Fig. 2. ^{31}P NMR spectra of TMPO adsorbed on (a) the pristine $H_3PW_{12}O_{40}$, various $[PheH]^+$-exchanged TPA catalysts: (b) $[PheH]H_2PW_{12}O_{40}$, (c) $[PheH]_2HPW_{12}O_{40}$, (d) $[PheH]_3PW_{12}O_{40}$, and (e) the bulk Phe.

The morphologies of various $(PheH)_xH_{3-x}PW_{12}O_{40}$ (x=1-3) composite catalysts were investigated by FE-SEM measurements. As illustrated in Fig. 3, the fully substituted $[PheH]_{3.0}PW_{12}O_{40}$ sample (x=3; Fig. 3(b)) exhibited better crystallinity than its $[PheH]_{1.0}H_{2.0}PW_{12}O_{40}$ counterpart with x=1 (Fig. 3(a)). These results coincide with those obtained from XRD measurements (Fig. S3; SI), revealing the increase in sample crystallinity with increasing Phe concentration.

2. Catalytic Performances

The oxidation of BzOH with H_2O_2 over various amino acid-modified TPA, *viz.* $[MH]_xH_{3-x}PW_{12}O_4$ (M=Phe, Ala, Gly; x=1-3) were conducted under the reaction conditions: $BzOH/H_2O_2$=1 : 2 (mol/mol), catalyst amount=6 wt%, water amount=30 mL, reaction time=4 h, and temperature=110 °C. The catalytic performances in terms of BzOH conversion, and product (*i.e.*, BzH) selectivity and yield are depicted in Table 1. For comparison, the catalytic activity over the bulk Phe and the pristine TPA were also evaluated. Unlike bulk Phe, which showed null conversion and BzH yield, the pristine TPA exhibited a satisfactory conversion of 96.7% and product selectivity and yield of 90.0% and 87%, respectively. Nonetheless, the $[MH]_xH_{3-x}PW_{12}O_4$ (M=Phe, Ala, Gly; x=1-3) composite catalysts showed even better activity with conversion≥96.3%, selectivity≥91.8, and yield≥88.4%, even though the pristine TPA was found to possess the strongest Brønsted acidity (*vide supra*). Clearly, catalysts with ultra-strong Brønsted acidity are not readily favorable for catalytic oxidation of alcohol. Among various composite catalysts examined, the $[PheH]_xH_{3-x}PW_{12}O_{40}$ catalyst with x=1 (*i.e.*, $[PheH]H_2PW_{12}O_{40}$) exhibited the best catalytic activity (conversion 97.9%, selectivity 97.4%, and yield 95.4%). Compared with its Phe-functionalized TPA counterparts, the $[PheH]H_2PW_{12}O_{40}$ being with the most available (two) Brønsted acidic protons (hence strongest acidity) show superior activity compared to

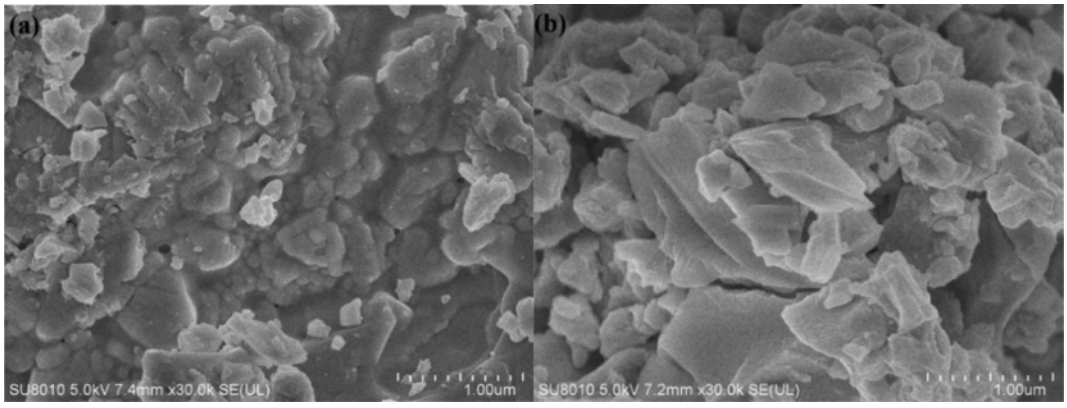

Fig. 3. FE-SEM images of (a) $[PheH]H_2PW_{12}O_{40}$, and (b) $[PheH]_3PW_{12}O_{40}$ catalyst samples.

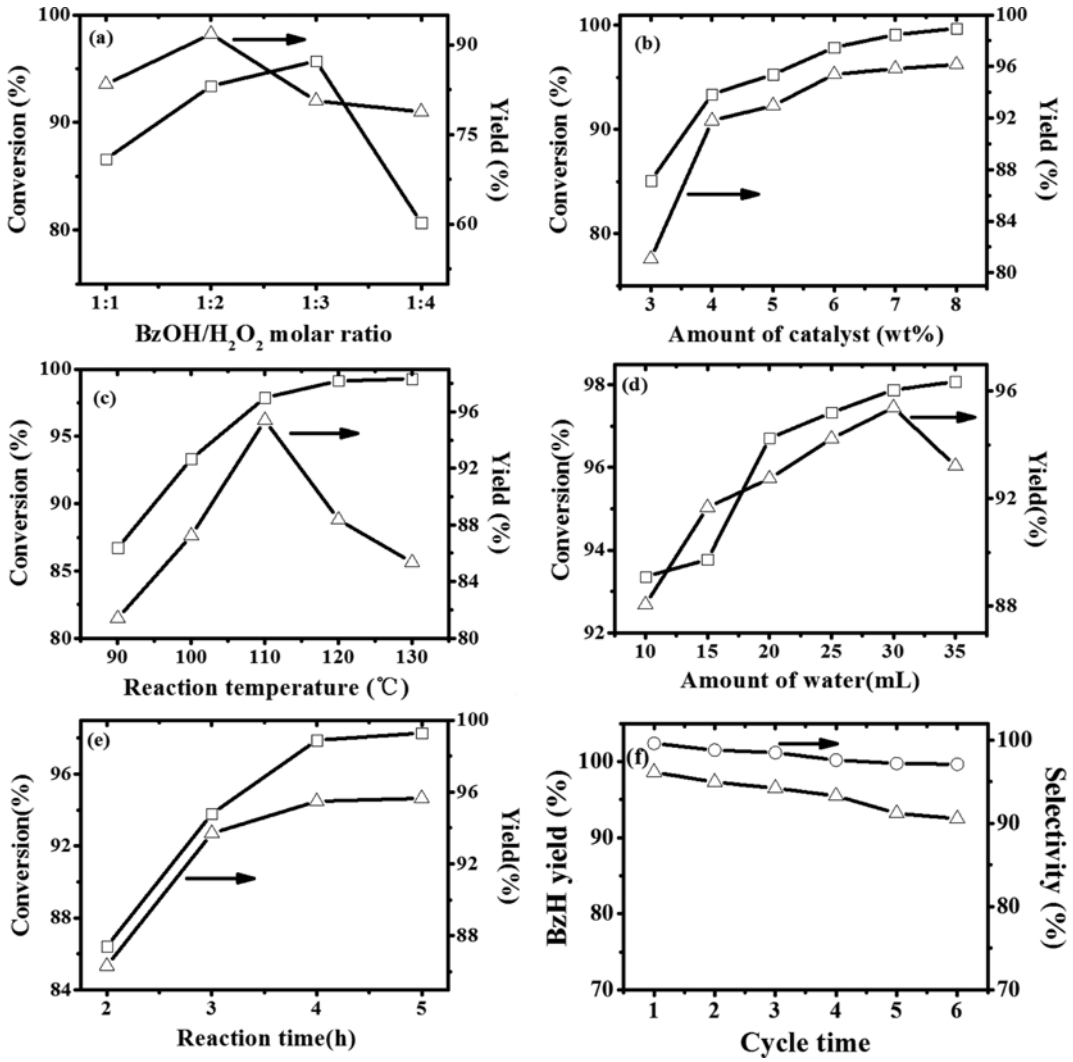

Fig. 4. Variations of conversion (□) and yield (△) influenced by individual experimental variable: (a) $BzOH/H_2O_2$ molar ratio, (b) catalysts loading, (c) reaction temperature, (d) amount of water, and (e) reaction time during oxidation of BzOH with H_2O_2 over the $[PheH]H_2PW_{12}O_{40}$ catalyst. (f) Variations of product yield and selectivity over catalyst recycle time; reaction conditions: $BzOH/H_2O_2$=1.0 : 1.5 (mol/mol); reaction time=3.8 h; amount of catalyst=6.1 wt%; amount of water=30.2 mL; temperature=110 °C.

$[PheH]_2HPW_{12}O_{40}$ (one residual H^+) and $[PheH]_3PW_{12}O_{40}$. The latter with null residual proton (hence weakest acidity) gave rise to inferior catalytic performances for oxidation of BzOH (see Table 1). On the other hand, comparing $[MH]H_2PW_{12}O_{40}$ with M=Phe with its counterparts with M=Ala and Gly; their catalytic activity follow the trend: $[PheH]_2HPW_{12}O_{40}$>$[AlaH]_2HPW_{12}O_{40}$>$[GlyH]_2HPW_{12}O_{40}$. In an earlier work, we have demonstrated that $[GlyH]H_2PW_{12}O_{40}$, which has a stronger Brønsted acidity than $[PheH]H_2PW_{12}O_{40}$, showed excellent catalytic activity during esterification of palmitic acid to biodiesel [29]. Thus, it is indicative that a stronger overall acidity of the catalyst is preferred for esterification than catalytic oxidation, which requires only a modest acidity.

3. Effects of Experimental Variables on Oxidation of Alcohol

The effects of experimental variables, *e.g.*, alcohol to oxidant ($BzOH/H_2O_2$) molar ratio, amount of catalyst, amount of water, reaction temperature, and time, on catalytic activity during oxidation of BzOH to BzH were investigated. The $[PheH]_2HPW_{12}O_{40}$ catalyst, which showed the best catalytic activity (*vide supra*), was used for the study.

The influence of relative alcohol to oxidant amounts was assessed by varying the molar ratio of $BzOH/H_2O_2$ while keeping other experimental variables fixed: *viz.* catalyst loading=4 wt%, reaction temperature=110 °C, amount of water=30 mL, and reaction time=4 h. As shown in Fig. 4(a), the conversion of BzOH increased with increasing $BzOH/H_2O_2$ molar ratio, reaching a maximum (95.71) at a ratio of 1 : 3. Clearly, a surplus amount of H_2O_2 oxidant is favorable for shifting the equilibrium towards formation of BzH. Meanwhile, an optimal BzH yield of 91.8% was obtained at a $BzOH/H_2O_2$ ratio of 1 : 2. Nevertheless, further increasing the amount of H_2O_2 led to inferior BzOH conversion and BzH product yield most likely due to undesirable dilution of the alcohol reactant and catalyst.

The effect of catalyst amount on oxidation of BzOH were studied by varying the catalyst loading from 3 to 8 wt% while main-

taining the other experimental parameters fixed: *viz.* BzOH/H_2O_2 ratio=1 : 2, reaction temperature=110 °C, amount of water=30 mL, and reaction time=4 h. Notable increases in both BzOH conversion and BzH yield with increasing catalyst amount were evident, and gradually reached a respective plateau when the catalyst loading exceeded *ca.* 6 wt% (Fig. 4(b)). This is ascribed to the increase in available acid sites with increasing catalyst loading for catalyzing the oxidation reaction. For this reason as well as economical viewpoint, a catalyst amount of 6 wt% was chosen for subsequent study even though a slightly higher BzOH conversion and BzH yield were obtained with a catalyst amount of 8 wt%.

Since reaction temperature has a great influence on reaction rate and reaction activity (*i.e.*, conversion and selectivity), its effect on oxidation of alcohol was also investigated. This is accomplished by varying the reaction temperature from 90 to 130 °C while fixing other experimental parameters (*viz*, BzOH/H_2O_2 ratio=1 : 2, amount of catalyst=6 wt%, amount of water=30 mL, and reaction time=4 h). The experimental results are displayed in Fig. 4(c). As expected, the conversion increased progressively with increasing reaction temperature due to corresponding increase in reaction rate. However, a maximum BzH yield of 95.4% was observed at 110 °C, further increase in reaction temperature led to a drastic decrease in product selectivity. This is attributed to the increasing occurrence of side reactions at higher reaction temperatures by which the product selectivity was spoiled by the presence of undesirable by-products. For this reason, a reaction temperature of 110 °C was chosen for subsequent studies. Similarly, the BzOH conversion was found to increase consistently with increasing amount of water in the reaction system, leading to an optimal BzH selectivity (95.4%) and a conversion of 97.9% at an amount of 30 mL (Fig. 4(d)). Clearly, the presence of suitable amount of water is favorable for adsorption and/or activation of oxidant, however, an excessive amount of water tends to dilute the reaction system, leading to inferior catalytic activity.

On the basis of experimental results described above, the effect of reaction time was also investigated. As shown in Fig. 4(e), both the BzOH conversion and BzH yield increased gradually with increasing time, and eventually reached their respective plateaus (conversion and yield *ca.* 97.9 and 95.4%, respectively) as the reaction time reached 4 h. Thus, it is indicative that, over the $[PheH]_2HPW_{12}O_{40}$ organic-inorganic composite catalyst, best catalytic performances during oxidation of BzOH with H_2O_2 may be achieved under the following optimal experimental conditions: BzOH/H_2O_2 ratio=1 : 2, reaction temperature=110 °C, catalyst amount=6 wt%, amount of water=30 mL, and reaction time=4 h.

4. Process Optimization and Model Analysis

Factorial design of experiments and response surface methodology (RSM) were exploited to evaluate the interactive effects between pairs of experimental variables and to optimize the reaction conditions for the best benzaldehyde (BzH) yield during the oxidation of benzyl alcohol (BzOH) over the most prominent amino acid-modified TPA catalyst, namely $[PheH]_2HPW_{12}O_{40}$, which exhibited the best catalytic activity. Moreover, the analysis of variance (ANOVA) method was adopted to evaluate the influence of process variables on catalytic reaction as well as validity and significant of the proposed model. The representative symbols of various experimental variables and their corresponding coded levels and ranges are depicted in Table 2. By means of multiple regression analysis, the response (i.e., benzaldehyde yield), Y, which may be correlated with independent experimental variables by a qua-

Table 4. List of results obtained from ANOVA for the benzaldehyde yield

Source	Sum of square	DF[a]	Mean square	F	*Prob>F*	Signif.[b]
Model	3669.71	14	262.12	50.33	<0.0001	**
x_1	2347.80	1	2347.80	450.79	<0.0001	**
x_2	3.99	1	3.99	0.77	0.3962	
x_3	169.35	1	169.35	32.52	<0.0001	**
x_4	72.57	1	72.57	13.93	0.0022	**
x_1^2	912.54	1	812.84	175.21	<0.0001	**
x_2^2	29.08	1	13.65	5.58	0.0331	
x_3^2	41.18	1	52.80	7.91	0.0138	*
x_4^2	52.08	1	65.05	10.00	0.0069	*
$x_1 x_2$	1.80	1	1.80	0.34	0.5664	
$x_1 x_3$	79.74	1	79.74	15.31	0.0016	**
$x_1 x_4$	38.38	1	38.38	7.37	0.0168	*
$x_2 x_3$	0.62	1	0.62	0.12	0.7344	
$x_2 x_4$	12.67	1	12.67	2.43	0.1411	
$x_3 x_4$	27.25	1	27.25	5.23	0.0383	*
Residual	72.91	14	5.21			
Lack of fit	64.28	10	6.43	2.98	0.1521	NS
Pure error	8.63	4	2.16			
Cor. total	3742.62	28				

[a]DF=degree of freedom

[b]Definition of symbols: *significant; **highly significant; NS=non-significant

dratic model based on Eq. (3) may be expressed as:

$$Y=95.48-13.32x_1+0.58x_2-3.76x_3+2.46x_4 -11.19x_1^2-1.45x_2^2-2.85x_3^2-3.17x_4^2 +0.67x_1x_2-4.47x_1x_3+3.10x_1x_4+0.39x_2x_3+1.78x_2x_4+2.61x_3x_4 \quad (7)$$

where x_i (i=1-4) represent the experimental variables, namely BzOH/H_2O_2 molar ratio (x_1), amount of catalyst (x_2), reaction time (x_3), and amount of water (x_4), respectively. Their corresponding coded values and responses derived from Eqs. (2) and (7), respectively, are depicted in Table 3.

In general, the coefficient of determination (R^2) associated with the regression of Eq. (7) is used to assess the validity of the model. That a R^2 value of 0.9805 was obtained for the model, indicating that at least 98.05% of the experimental data could be explained by the proposed model. As depicted in Table 4, the obtained coefficient of variation (CV) value of 2.61 reveals the precision of the model and reliability of process optimization. An *F*-value of 2.98 was obtained, implying that the "Lack of Fit" was insignificant. On the other hand, a model *F*-value and a *Prob>F* values of 50.33 and <0.050 were obtained, respectively, indicating that the model and associated terms were both significant. In this context, model terms such as x_1, x_3, x_4, x_1^2, x_2^2, x_3^2, x_4^2, x_1x_3, x_1x_4, and x_3x_4 may be considered significant.

The two-dimensional (2D) contour plots between each pair of experimental variables and corresponding three-dimensional (3D) response surface plots obtained from the predicted model are also displayed in Figs. S5 and S6 (SI), respectively. Accordingly, it may be inferred that correlations between BzOH/H_2O_2 molar ratio (x_1) and reaction time (x_3) are highly significant, consistent with the low *Prob>F* value observed (0.0016). The nearly elliptical shape of the contour plots in Figs. S5 ((c) and (f); SI) indicate a strong correlation between the amount of water (x_4) with BzOH/H_2O_2 ratio (x_1) and reaction time (x_3), respectively. On the other hand, the nearly circular shape and scattered contour plots in Figs. S5 ((a), (d), and (e); SI) reveal that the correlations between the catalyst amount (x_2) with the other three variables are all insignificant. These findings are consistent with the ANOVA data listed in Table 4.

On the basis of the RSM results, the mathematical model in Eq. (7) predicted an optimal BzH yield (Y) of 99.76% for oxidation of BzOH over the [PheH]$H_{2.0}PW_{12}O_{40}$ catalyst under the following process conditions: BzOH/H_2O_2 molar ratio (x_1)=1 : 1.46 mol/mol, amount of catalyst (x_2)=6.05 wt%, reaction time (x_3)=3.75 h, and amount of water (x_4)=30.22 mL at a reaction temperature of 110 °C. To verify the validity of the model and optimized process conditions, three additional experiments were performed in parallel using the more realistic reaction conditions: x_1=1 : 1.5 mol/mol, x_2=6.1 wt%, x_3=3.8 h, and x_4=30.2 mL. As a result, an experimental BzH yield of 98.6% with a BzOH conversion of 99.0% corresponding to BzH selectivity of 99.6% were obtained, in good agreement with the predicted value.

5. Catalyst Recycling

The recyclability of the [PheH]$H_2PW_{12}O_{40}$ catalyst for oxidation of BzOH with H_2O_2 under the optimal process conditions, *viz.* BzOH/H_2O_2=1 : 1.5 (mol/mol), reaction time=3.8 h, amount of catalyst=6.1 wt%, amount of water=30.2 mL, and temperature=110 °C, was tested. After each run, the catalyst was washed by diethyl ether and reused after drying under vacuum for 8 h at 70 °C. As shown in Fig. 4(f), the [PheH]$H_2PW_{12}O_{40}$ catalyst showed excellent stability and recyclability with only slight decreases in BzOH conversion (from 99.0% to 95.3%) and BzH yield (from 98.6 to 92.5%) and marginal change in selectivity (from 99.6 to 97.1%) after six repeated cycles. Additional evidences from FT-IR measurements revealed that the structural integrity of the catalyst remained practically unchanged even after six consecutive runs; the characteristic absorption bands responsible for the Keggin polyanions (PW; $PW_{12}O_{40}^{3-}$) of TPA remained practically intact (Fig. S7; SI). The above results clearly indicate that the [PheH]$H_2PW_{12}O_{40}$ catalyst is rather durable during catalytic oxidation reaction; majority of the active species in the spent catalyst may be regenerated for catalytic recycling, hence, favorable for practical industrial applications.

6. Kinetic Modelling

The kinetic model for the oxidation of BzOH with H_2O_2 to BzH over the [PheH]$H_2PW_{12}O_{40}$ catalyst was established based on the rate equation in Eqs. (4) and (5). Accordingly, the reaction order corresponds to the reactant (BzOH; denoted as α) and oxidant (H_2O_2; denoted as β) may be derived together with the activation energy (E_a) and pre-exponential factor (k_0) of the reaction system defined in Eq. (6).

To afford derivation of reaction orders (α and β), reactions were conducted by varying the concentration of either BzOH or H_2O_2 while keeping its counterpart constant. For examples, reactions were carried out by varying the initial BzOH concentrations (from 1.16 to

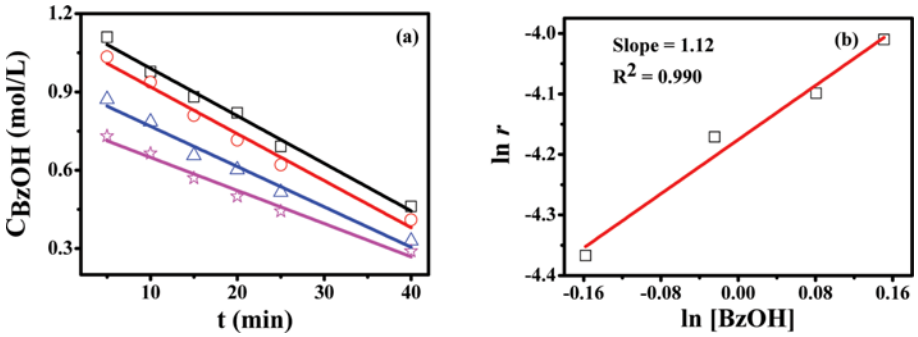

Fig. 5. (a) Variations of BzOH concentration vs reaction time under different initial concentrations [BzOH]=1.16 (□), 1.08 (○), 0.98 (△), and 0.85 (☆) mol/L, and (b) log-log plot of initial oxidation rate (r) vs initial [BzOH]; reaction conditions: temperature=110 °C; initial [H_2O_2]=1.70 mol/L; [BzH]=0 mol/L; amount of catalyst=7.79 g/L.

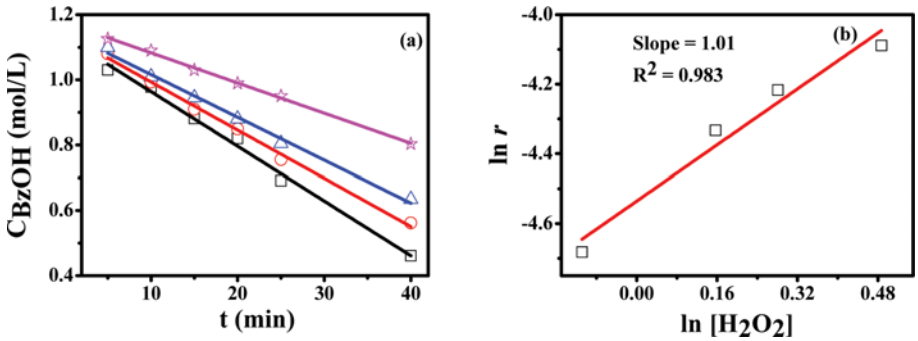

Fig. 6. (a) Variations of H_2O_2 concentration vs reaction time under different initial concentrations [H_2O_2]: 1.63 (□), 1.33 (○), 1.17 (△), and 0.90 (☆) mol/L, and (b) log-log plot of initial oxidation rate (r) vs initial [H_2O_2]; reaction conditions: temperature=110 °C; initial [BzOH]=1.16 mol/L; [BzH]=0 mol/L; amount of catalyst=7.79 g/L.

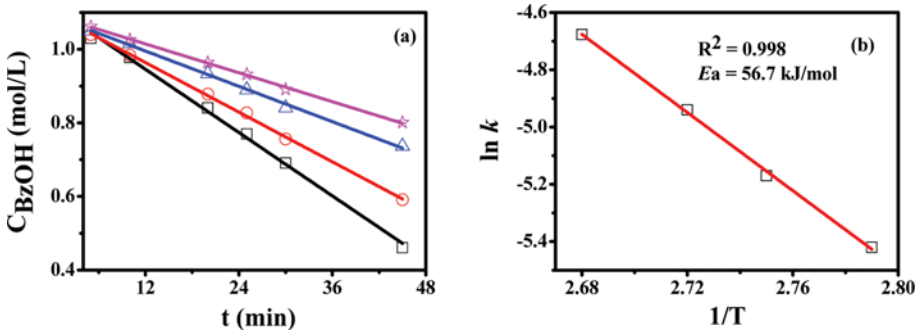

Fig. 7. (a) Variations of BzOH concentration vs reaction time under different reaction temperatures: 383 K (□), 378 K (○), 373 K (△), and 368 K (☆), and (b) the corresponding Arrhenius plot; reaction conditions: initial [BzOH]=1.16 mol/L; [H_2O_2]=1.63 mol/L; amount of catalyst=7.79 g/L.

0.85 mol/L) while keeping the concentrations of H_2O_2 (1.70 mol/L), desirable amount of water, over a fixed amount of [PheH]$H_2PW_{12}O_{40}$ catalyst (7.79 mol/L) at constant temperature (110 °C). The reaction rate r for oxidation of BzOH with H_2O_2 to BzH may be defined based on Eq. (5), as shown in Fig. 5(a). Accordingly, a reaction order (α) of *ca.* 1.12 may be derived, as shown in in Fig. 5(b). Similarly, by changing the concentrations of H_2O_2 (from 1.63 to 0.90 mol/L; Fig. 6(a)), while maintaining the other parameters fixed, the reaction order for H_2O_2 (β) was found to be ca. 1.01 (Fig. 6(b)).

Taking the optimal reaction conditions predicted by RSM, *viz.*, BzOH/H_2O_2=1 : 1.5 mol/mol, amount of catalyst=6.1 wt%, reaction time=3.8 h, and amount of water=30.2 mL, while varying the reaction temperature from 95 to 110 °C (see Fig. 7(a)), an activation energy E_a=56.7 kJ mol^{-1} was obtained (Fig. 7(b)); a value which is much lower than that observed for a manganese oxide catalyst (71.81 kJ/mol) during oxidation of BzOH using molecular oxygen (O_2) as the oxidant [40].

CONCLUSIONS

A series of novel amino acid-modified TPA ($H_3PW_{12}O_{40}$) hybrid materials, namely $[MH]_xH_{3-x}PW_{12}O_{40}$ (x=0-3) with M=phenylalanine (Phe), alanine (Ala), and glycine (Gly) were synthesized and applied as acid catalysts for oxidation of alcohol. Among them, the [PheH]$H_2PW_{12}O_{40}$ catalyst exhibited excellent thermal stability and desirable strong acidity to render a high catalytic activity during oxidation of benzyl alcohol with hydrogen peroxide. As a result, a high benzaldehyde yield of 98.6% was achieved with an alcohol conversion of 99.0%, which corresponding to an extraordinary high product selectivity of 99.6% were achieved. The [PheH]$H_2PW_{12}O_{40}$ catalyst was also found to be durable and recyclable with only marginal decrease in catalytic activity after six consecutive runs. Moreover, the alcohol oxidation reaction over the composite salt was found to have an lower activation energy than typical solid acid catalysts. Thus, such organic-inorganic composite materials, which exhibit exotic properties such as strong acidity, thermal stability, durability, and recyclability represent eco-friendly and cost-effective heterogeneous catalysts that are feasible for large-scale production and practical industrial applications.

ACKNOWLEDGEMENTS

The supports of this work by Science and Technology Department of Zhejiang Province (No. 2016C31016) and Program for Zhejiang Leading Team of S & T Innovation (No. 2013TD07), China, and the Ministry of Science and Technology, Taiwan (MOST 104-2113-M-001-019) are gratefully acknowledged.

SUPPORTING INFORMATION

Additional information as noted in the text. This information is

available via the Internet at http://www.springer.com/chemistry/journal/11814.

REFERENCES

1. D. I. Enache, J. K. Edwards, P. Landon, B. Solsona-Espriu, A. F. Carley, A. A. Herzing, M. Watanabe, C. J. Kiely, D. W. Knight and G. J. Hutchings, *Science*, **311**, 362 (2006).
2. Y. Pérez, R. Ballesteros, M. Fajardo, I. Sierra and I. del Hierro, *J. Mol. Catal. A*, **352**, 45 (2012).
3. P. Sudarsanam, B. Mallesham, D. Naga Durgasri and B. M. Reddy, *J. Ind. Eng. Chem.*, **20**, 3115 (2014).
4. J. U. Ahmad, M. T. Räisänen, M. Leskelä and T. Repo, *Appl. Catal. A*, **411-412**, 180 (2012).
5. V. Cortés Corberán, M. E. González-Pérez, S. Martínez-González and A. Gómez-Avilés, *Appl. Catal. A*, **474**, 211 (2014).
6. D. Qiao, C. Xu and J. Xu, *Catal. Commun.*, **45**, 44 (2014).
7. Y. Zhou, G. Chen, Z. Long and J. Wang, *RSC Adv.*, **4**, 42092 (2014).
8. M. R. Farsani, F. Jalilian, B. Yadollahi and H. A. Rudbari, *Polyhedron*, **76**, 102 (2014).
9. W. Zhao, Y. Zhang, B. Ma, Y. Ding and W. Qiu, *Catal. Commun.*, **11**, 527 (2010).
10. C. N. Kato, M. Nagami and N. Ukai, *Appl. Catal. A*, **452**, 69 (2013).
11. L. Zhou, E. Al-Zaini and A. A. Adesina, *Fuel*, **103**, 617 (2013).
12. Ch. Ramesh Kumar, K. T. Venkateswara Rao, P. S. Sai Prasad and N. Lingaiah, *J. Mol. Catal.* A, **337**, 17 (2011).
13. A. Ghanbari-Siahkali, A. Philippou, J. Dwyer and M. W. Anderson, *Appl. Catal. A*, **192**, 57 (2000).
14. P. Madhusudhan Rao, A. Wolfson, S. Kababya, S. Vega and M. V. Landau, *J. Catal.*, **232**, 210 (2005).
15. X. Han, W. Yan, K. Chen, C. T. Hung, L. L. Liu, P. H. Wu, S. J. Huang and S. B. Liu, *Appl. Catal. A*, **485**, 149 (2014).
16. Ch. Ramesh Kumar, M. Srinivas and N. Lingaiah, *Appl. Catal. A*, **487**, 165 (2014).
17. Z. Liu, S. Cao, S. Wang, W. Zeng and T. Zhang, *Reac. Kinet. Mech. Cat.*, **111**, 577 (2014).
18. J. Pandey and A. Shukla, *Solid State Ionics*, **262**, 811 (2014).
19. G. Luo, L. Kang, M. Zhu and B. Dai, *Fuel Process. Technol.*, **118**, 20 (2014).
20. M. Y. Huang, X. X. Han, C. T. Hung, J. C. Lin, P. H. Wu, J. C. Wu and S. B. Liu, *J. Catal.*, **320**, 42 (2014).
21. X. Dong, D. Wang, K. Li, Y. Zhen, H. Hu and G. Xue, *Mater. Res. Bull.*, **57**, 210 (2014).
22. S. Pathan and A. Patel, *Appl. Catal. A*, **459**, 59 (2013).
23. S. S. Wang, J. Zhang, C. L. Zhou, G. Vo-Thanh and Y. Liu, *Catal. Commun.*, **28**, 152 (2012).
24. D. R. Park, J. H. Choi, S. Park and I. K. Song, *Appl. Catal. A*, **394**, 201 (2011).
25. Z. Sun, S. Wang, X. Wang and Z. Jiang, *Fuel*, **164**, 262 (2016).
26. Y. Leng, P. Zhao, M. Zhang and J. Wang, *J. Mol. Catal. A*, **358**, 67 (2012).
27. N. R. Shiju, A. H. Alberts, S. Khalid, D. R. Brown and G. Rothenberg, *Angew. Chem. Int. Ed.*, **50**, 9615 (2011).
28. N. A. Brunelli, S. A. Didas, K. Venkatasubbaiah and C. W. Jones, *J. Am. Chem. Soc.*, **134**, 13950 (2012).
29. Y. Yang, X. Liu, X. Li, J. Zhao, S. Bai, J. Liu and Q. Yang, *Angew. Chem. Int. Ed.*, **51**, 9164 (2012).
30. X. Han, K. Chen, W. Yan, C. T. Hung, L. L. Liu, P. H. Wu, K. C. Lin and S. B. Liu, *Fuel*, **165**, 115 (2016).
31. A. Zheng, S. J. Huang, S. B. Liu and F. Deng, *Phys. Chem. Chem. Phys.*, **13**, 14889 (2011).
32. A. Zheng, S. Li, S. B. Liu and F. Deng, *Acc. Chem. Res.*, **49**, 655 (2016).
33. Y. Zubavichus, M. Zharnikov, A. Shaporenko, O. Fuchs, L. Weinhardt, C. Heske, E. Umbach, J. D. Denlinger and M. Grunze, *J. Phys. Chem. A*, **108**, 4557 (2004).
34. I. V. Kozhevnikov, S. Holmes and M. R. H. Siddiqui, *Appl. Catal. A*, **214**, 47 (2001).
35. M. S. Akhtar, K. K. Cheralathan, J. M. Chun and O. B. Yang, *Electrochim. Acta*, **53**, 6623 (2008).
36. S. J. Huang, C. Y. Yang, A. Zheng, N. Feng, N. Yu, P. H. Wu, Y. C. Chang, Y. C. Lin, F. Deng and S. B. Liu, *Chem. Asian J.*, **6**, 137 (2011).
37. R. Mahalakshmi, S. X. Jesuraja and S. Jerome Das, *Cryst. Res. Technol.*, **41**, 780 (2006).
38. A. Zheng, S. J. Huang, W. H. Chen, P. H. Wu, H. Zhang, H. K. Lee, L. C. de Ménorval, F. Deng and S. B. Liu, *J. Phys. Chem. A*, **112**, 7349 (2008).
39. X. Han, Y. He, C. T. Hung, L. L. Liu, S. J. Huang and S. B. Liu, *Chem. Eng. Sci.*, **104**, 64 (2013).
40. M. Saeed, M. Ilyas and M. Siddique, *Int. J. Chem. Kinet.*, **47**, 447 (2015).

Supporting Information

Heterogeneous amino acid-based tungstophosphoric acids as efficient and recyclable catalysts for selective oxidation of benzyl alcohol

Xiaoxiang Han[*,†], Yingying Kuang[*], Chunhua Xiong[*], Xiujuan Tang[**], Qing Chen[*], Chin-Te Hung[***], Li-Li Liu[***], and Shang-Bin Liu[*,†]**

*Department of Applied Chemistry, Zhejiang Gongshang University, Hangzhou 310018, China
**College of Environmental Science and Engineering, Zhejiang Gongshang University, Hangzhou 310018, China
***Institute of Atom and Molecular Sciences, Academic Sinica, Taipei 10617, Taiwan
(*Received 29 November 2016 • accepted 4 April 2017*)

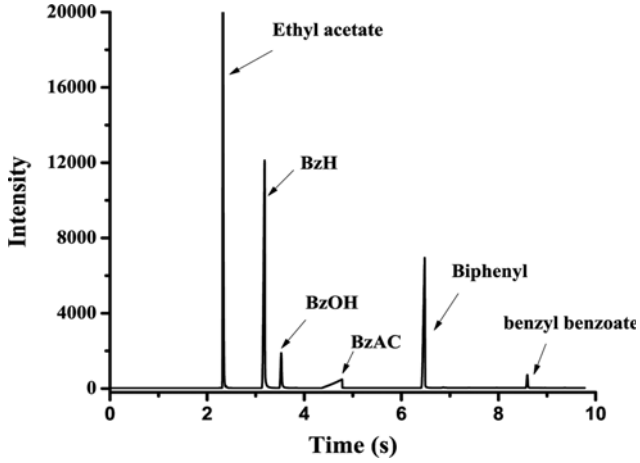

Fig. S1. Typical GC profile of primary products, namely ethyl acetate, benzaldehyde (BzH), benzyl alcohol (BzOH), benzyl acid (BzAC), biphenyl, and benzyl bemzoate.

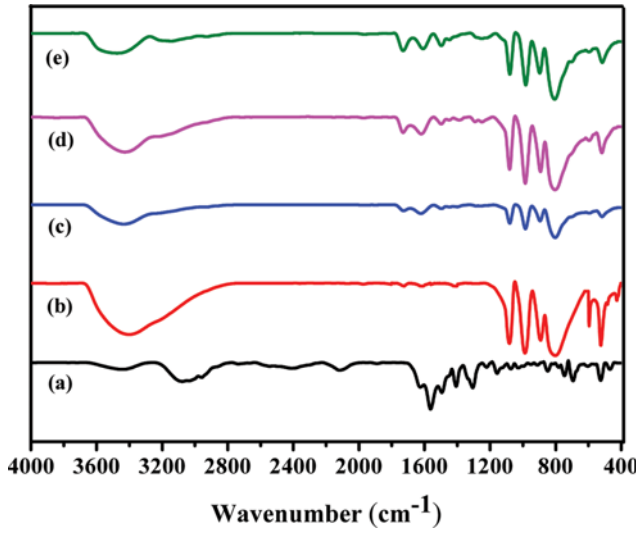

Fig. S2. FT-IR spectra of (a) bulke phenylalanine (Phe), (b) pristine TPA ($H_3PW_{12}O_{40}$), and Phe-modified TPA: (c) $[PheH]H_2PW_{12}O_{40}$, (d) $[PheH]_2HPW_{12}O_{40}$ and (e) $[PheH]_3PW_{12}O_{40}$.

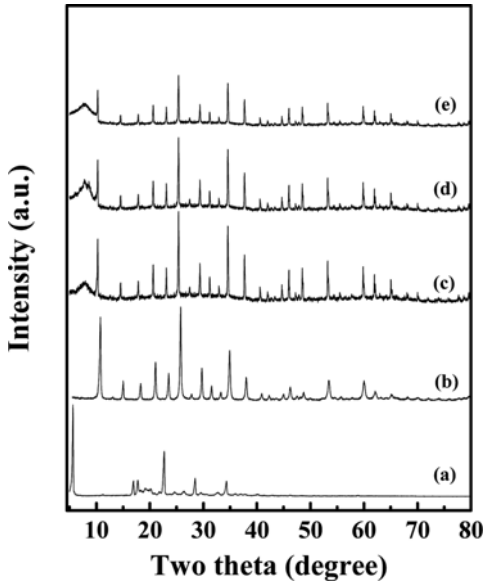

Fig. S3. XRD spectra of (a) bulk Phe, (b) pristine $H_3PW_{12}O_{40}$, (c) $[PheH]H_2PW_{12}O_{40}$, (d) $[PheH]_2HPW_{12}O_{40}$, and (e) $[PheH]_3PW_{12}O_{40}$.

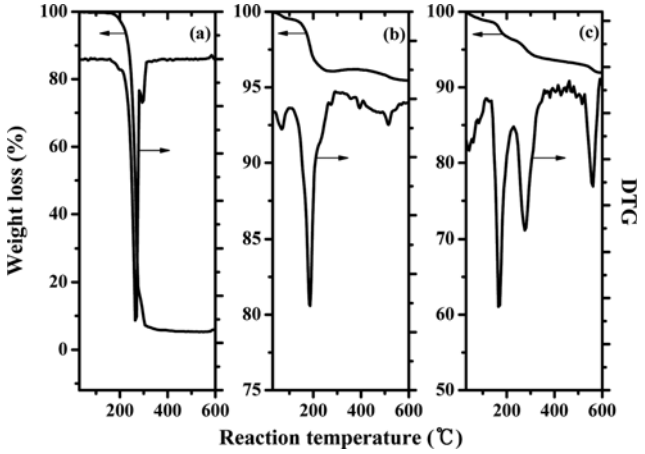

Fig. S4. TG-DTG profiles of the (a) bulk Phe, (b) pristine $H_3PW_{12}O_{40}$, and (c) $[PheH]H_2PW_{12}O_{40}$.

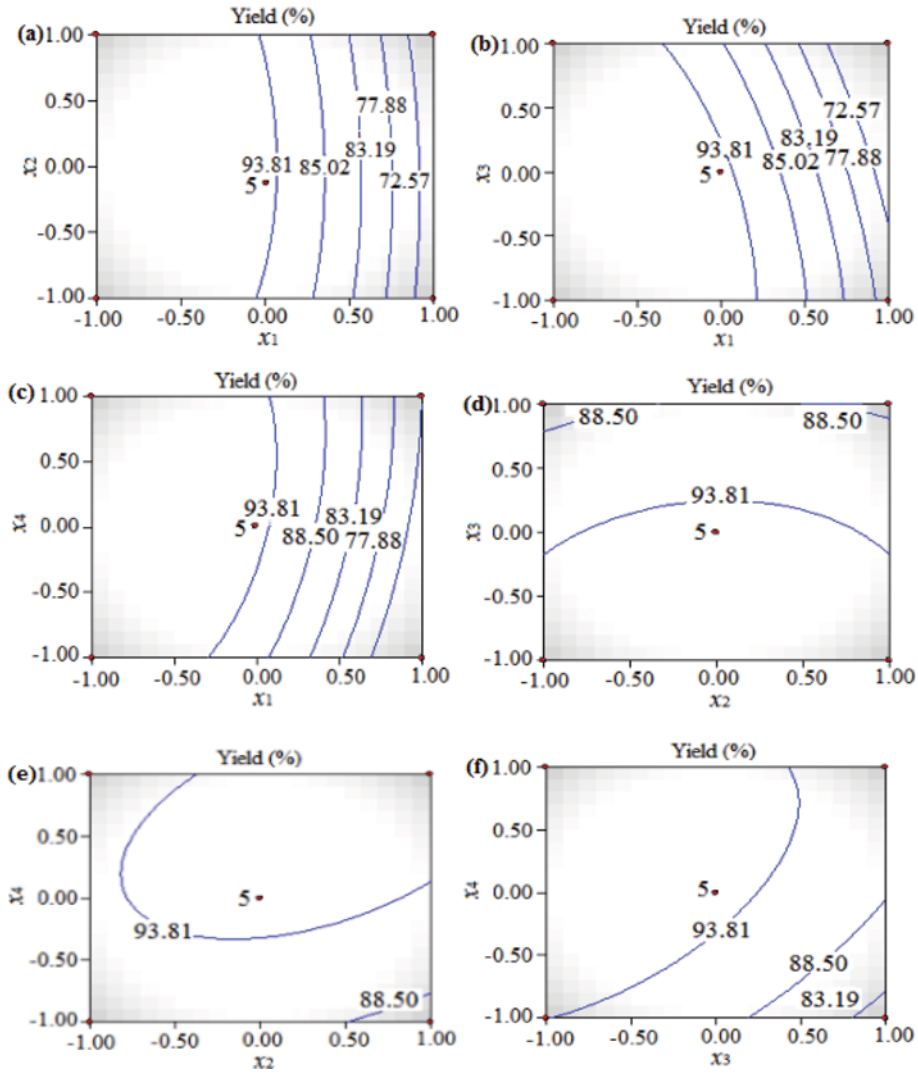

Fig. S5. Contour plots showing variations between a pair of experimental variables (see Table 2) on the predicted values of benzaldehyde (BzH) yield while keeping other variable at a constant level of 0. Notations: x_1=BzOH/H_2O_2 molar ratio, x_2=amount of catalyst, x_3=reaction time, x_4=amount of water.

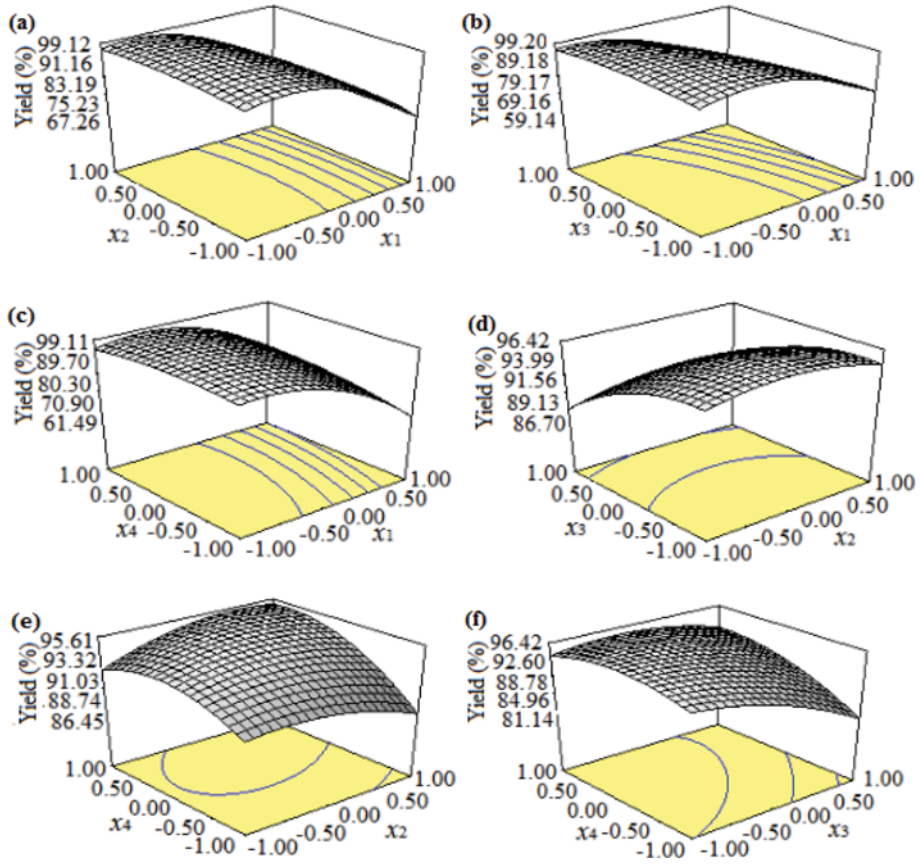

Fig. S6. Similar to Figure S5 but showing 3D response surface plots between a pair of experimental variables (see Table 2) on the predicted values of benzaldehyde yield while keeping other variable at a constant level of 0.

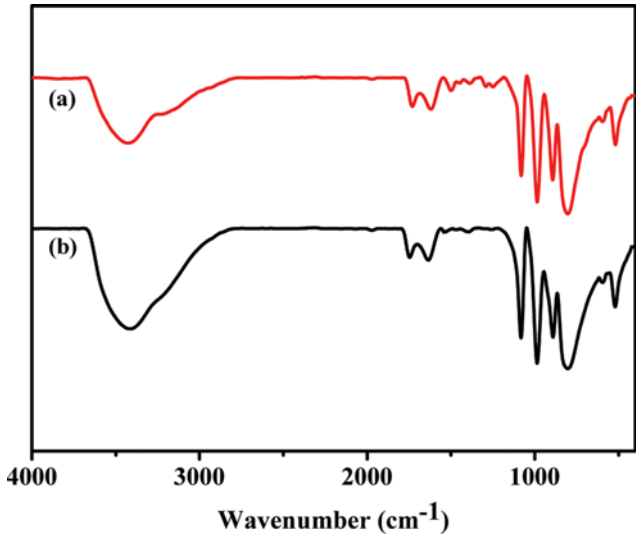

Fig. S7. FT-IR spectra of (a) the fresh and (b) the spent [PheH]H_2 $PW_{12}O_{40}$ catalyst regenerated after six consecutive runs.